Supporting Information

Dual active sites fabricated through atomic layer deposition of TiO_2 on MoS_2 nanosheet arrays for highly efficient electroreduction of CO_2 to ethanol

Feixuanyu Qi, ‡[ac] Kang Liu, ‡[b] De-Kun Ma,*[ac] Fangfang Cai,[c] Min Liu,*[b] Quanlong Xu,[c] Wei Chen,[c] Chenze Qi,[a] Dongpeng Yang [d] and Shaoming Huang *[d]

Experimental Section:

1.1 Materials and Chemicals

Ammonium tetrathiomolybdate (ATM, 99.95%), N, N-dimethylformamide (DMF, ≥99.9 %) and hydrazine monohydrate ($N_2H_2·H_2O$, >98.0%), analytical reagents of $KHCO_3$, acetone, and hydrochloric acid were purchased from Shanghai Aladdin Biochemical Technology Co. Ltd. Dimethylsulfoxide (DMSO) and ethanol (HPLC pure) were purchased from J&K chemicals. Mo mesh was purchased from Shengzhuo Stainless Steel Mesh Company. All chemicals were used without further purification. All the aqueous solutions were prepared with Milli Q water (18.2 MΩ cm). 1 × 4 cm^2 Mo mesh was washed with acetone, dilute hydrochloric acid, and high purity water before use.

1.2.1 Synthesis of ultrathin MoS_2 nanosheet arrays on Mo mesh

In a typical process, 10 mg of ATM was dissolved into 30 mL of DMF under ultrasonification. A piece of clean 1 × 4 cm^2 Mo mesh was put in the solution. Then 50 μl of $N_2H_4·H_2O$ was added to

the solution and stirred for 15 minutes. After that, it was transferred to a Teflon-lined stainless-steel autoclave, kept at 200 ^{o}C for 15 h. After the temperature cooled to room temperature, the Mo mesh containing MoS_2 was washed with highly purified water and dried at 65 ^{o}C under vacuum.

1.2. 2 Preparation of TiO_2/MoS_2

Different thickness of TiO_2 thin film was deposited upon the pre-prepared MoS_2/Mo with ALD system. The Titanium isopropoxide (TTIP) was used as Ti precursor, H_2O was used as an oxygen source. High-purity N_2 (99.999%) was used as the carrier gas with a flow of 100 sccm along the reactor. High-purity O_2 (99.999%) was used as the plasma gas with a flow of 300 sccm along the reactor. Each cycle of ALD deposits 0.4 Å of TiO_2. 25, 50, and 75 cycles were applied to obtained TiO_2 with thicknesses of 1, 2, and 3 nm, respectively.

1.3 Characterizations.

Powder X-ray diffraction (XRD) was carried out with a Bruker D8 Advance X-ray diffractometer using Cu Kα radiation (λ = 0.15418 nm) at a scanning rate of 7°/min in the 2θ range from 20° to 80°. Field emission scanning electron microscopy (FESEM) images were taken on a Nova NanoSEM 200 scanning electron microscope. Transmission electron microscopy (TEM) observations and high-resolution transmission electron microscope (HRTEM) images were performed with a JEOL JEM 2010 HRTEM, using an accelerating voltage of 200 kV. X-ray photoelectron spectra (XPS) were acquired on an ESCALAB 250 with Al Kα (hυ = 1253.6 eV) as the excitation source. The binding energies obtained in the XPS spectral analysis were corrected for specimen charging by referencing C 1s to 284.8 eV. The gaseous products from CO_2 electrochemical reduction were analyzed by gas chromatography (Agilent 7890A). The liquid products were analyzed by ^{1}H NMR spectroscopy (Bruker, 500M), with water suppression using a presaturation method.

1.4 Electrochemical measurements.

The electrocatalytic experiments were carried out through electrochemical workstation CHI760E in an H-type three-electrode electrochemical cell with 0.5 M $KHCO_3$ electrolyte saturated with Ar, CO_2, or CO. The working electrode and the anode compartment were separated by a cation exchange membrane (Nafion N115, DuPont). MoS_2/Mo and TiO_2/MoS_2 were used as working electrode.

Platinum plate and Ag/AgCl (in saturated KCl solution) electrode were used as the counter electrode and the reference electrode, respectively. The area of the cathode immersed in the electrolyte was confined to 1 × 1 cm^2. The voltage was applied from 0 to -1.2 V versus RHE. The scan rate was set as 5 mV s^{-1}. Cyclic voltammetry (CV) and linear sweep voltammetry (LSV) were performed to analyze the electrocatalytic activities of the as-obtained materials for CO_2RR. The electrochemical impendance spectra (EIS) were carried out at open circuit potential with an amplitude of 10 mV in a frequency range from 1 MHz to 10^{-2} Hz. The electrochemically active surface area (ECSA) was obtained through CV method. The specific capacitance was calculated by plotting the difference of the anodic and cathodic current densities at −0.1 V vs. RHE against the scan rate. Considering that flat sulfides electrode with 1 cm^2 has a specific capacitance of about 40 mF cm^{-2}, this value was also used to calculate ECSA of MoS_2 and TiO_2/MoS_2 electrodes through the following equation:

$$A_{ECSA} = \frac{Specific\ capacitance}{40\ \mu F cm^{-2} cm_{ECSA}^{-2}}$$

Computation method

Density functional theory (DFT) calculations were performed using the Vienna ab initio simulation package (VASP).[1] Electron-ion interactions were described using standard projector-augmented wave (PAW) potentials.[2] The generalized gradient approximation (GGA) with the Perdew-Burke-Ernzerhof (PBE) functional were used to describe the electron-electron exchange and correlation functional.[3] A plane wave cutoff energy of 400 eV was applied in our calculations. The spin polarization was considered in all calculation. The vacuum layer is 15 Å. The Brillouin-zone integrations were performed using the only Gama point during the optimization. The iterative process considered was convergences, when the force on the atom was less than 0.02 eV $Å^{-1}$ and the energy change was less than 10^{-5} eV per atom. van der Waals (VDW) interactions were corrected using the D2 method of Grimme.[4]

The computational hydrogen electrode (CHE) approach was used to calculate the free energy of all intermediate species. The formula is defined as

$$\Delta G = \Delta E + \Delta ZPE - T \times \Delta S$$

Where ΔE is the reaction energy calculated by the DFT method. ΔZPE and ΔS are the changes in zero-point energies and entropy during the reaction, respectively.[5]

Reference

[1] G. Kresse, J. Hafner, *Phys. Rev. B* **1994**, *49*, 14251–14269.

[2] P. E. Blöchl, *Phys. Rev. B* **1994**, *50*, 17953–17979.

[3] J. P. Perdew, K. Burke, M. Ernzerhof, *Phys. Rev. Lett*. 1996, 77, 3865–3868.

[4] S. Grimme, *J. Comput. Chem*. **2006**, *27*, 1787–1799.

[5] J. K. Nørskov, T. Bligaard, A. Logadottir, J. R. Kitchin, J. G. Chen, S. Pandelov. U. Stimming, *J. Electrochem. Soc*. **2005**, *152*, J23–J26.

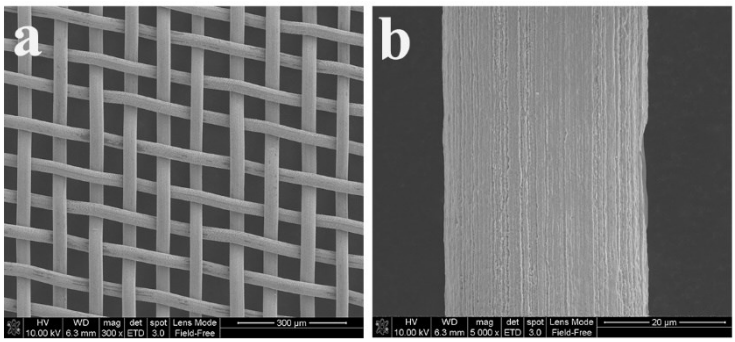

Fig. S1 FESEM images of the used Mo mesh at different magnification.

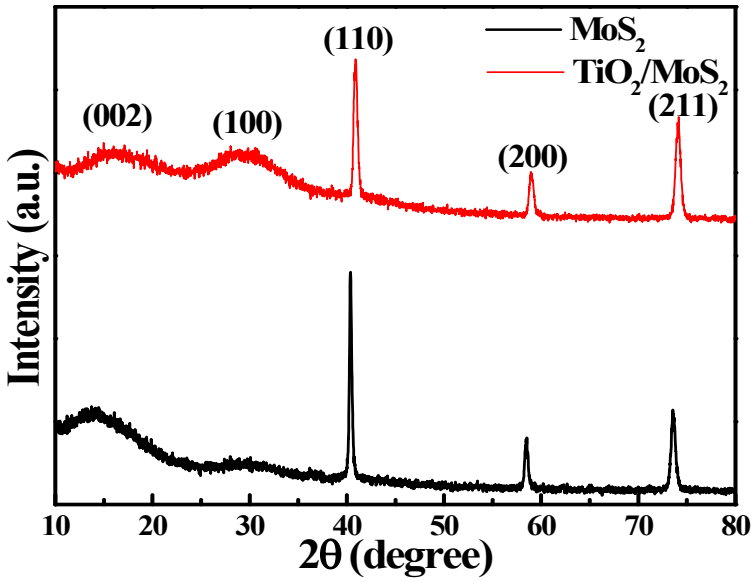

Fig. S2 XRD patterns of the as-synthesized MoS_2 nanosheet arrays and TiO_2/MoS_2.

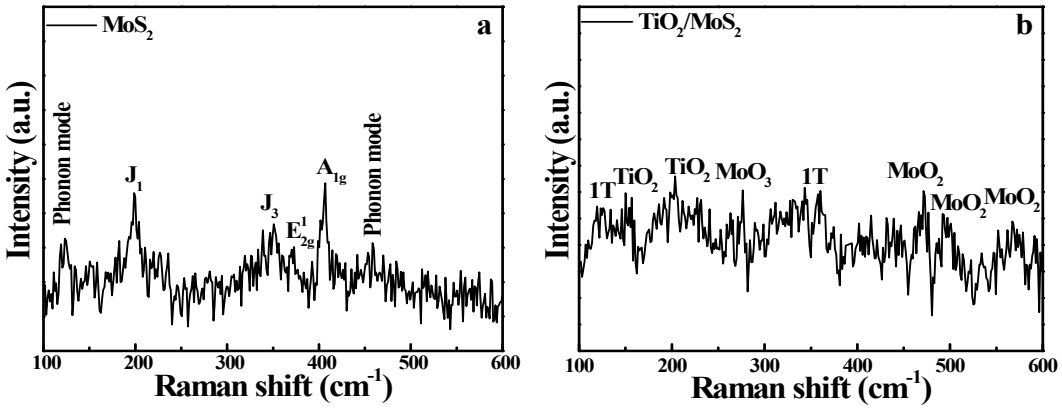

Fig. S3 Raman spectra of MoS_2 (a) and TiO_2/MoS_2 (b).

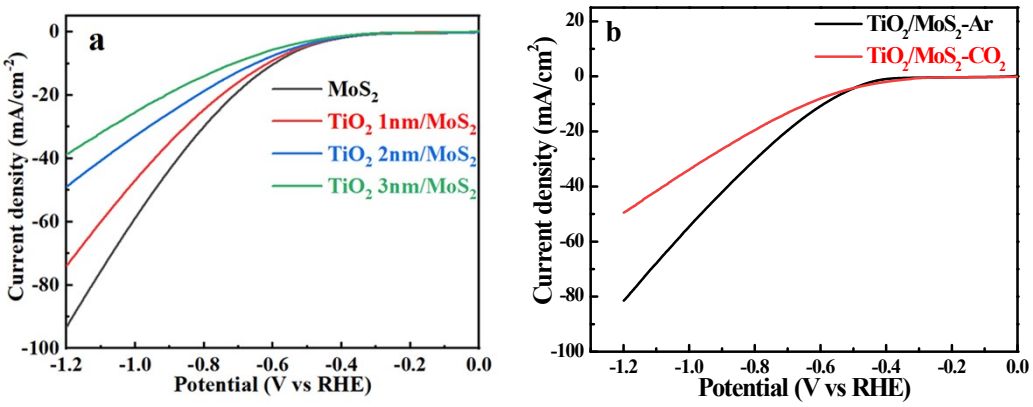

Fig. S4 LSV curves obtained over TiO_2 with different thicknesses/MoS_2 in CO_2-saturated 0.5 M $KHCO_3$ aqueous solution (a). LSV curves of 2 nm TiO_2/MoS_2 in Ar- and CO_2-saturated 0.5 M $KHCO_3$ aqueous solution (b).

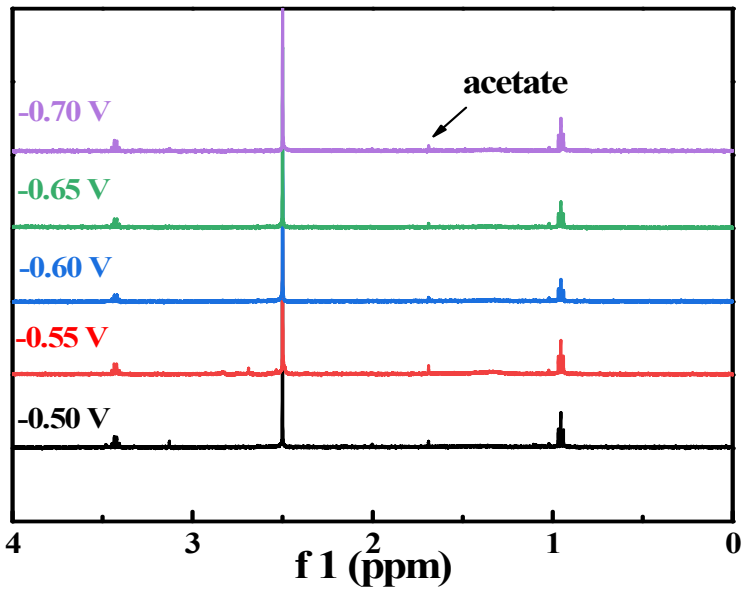

Fig. S5 ^1H NMR spectra of liquid products obtained through CO_2 electrolysis over TiO_2/MoS_2 nanosheet arrays.

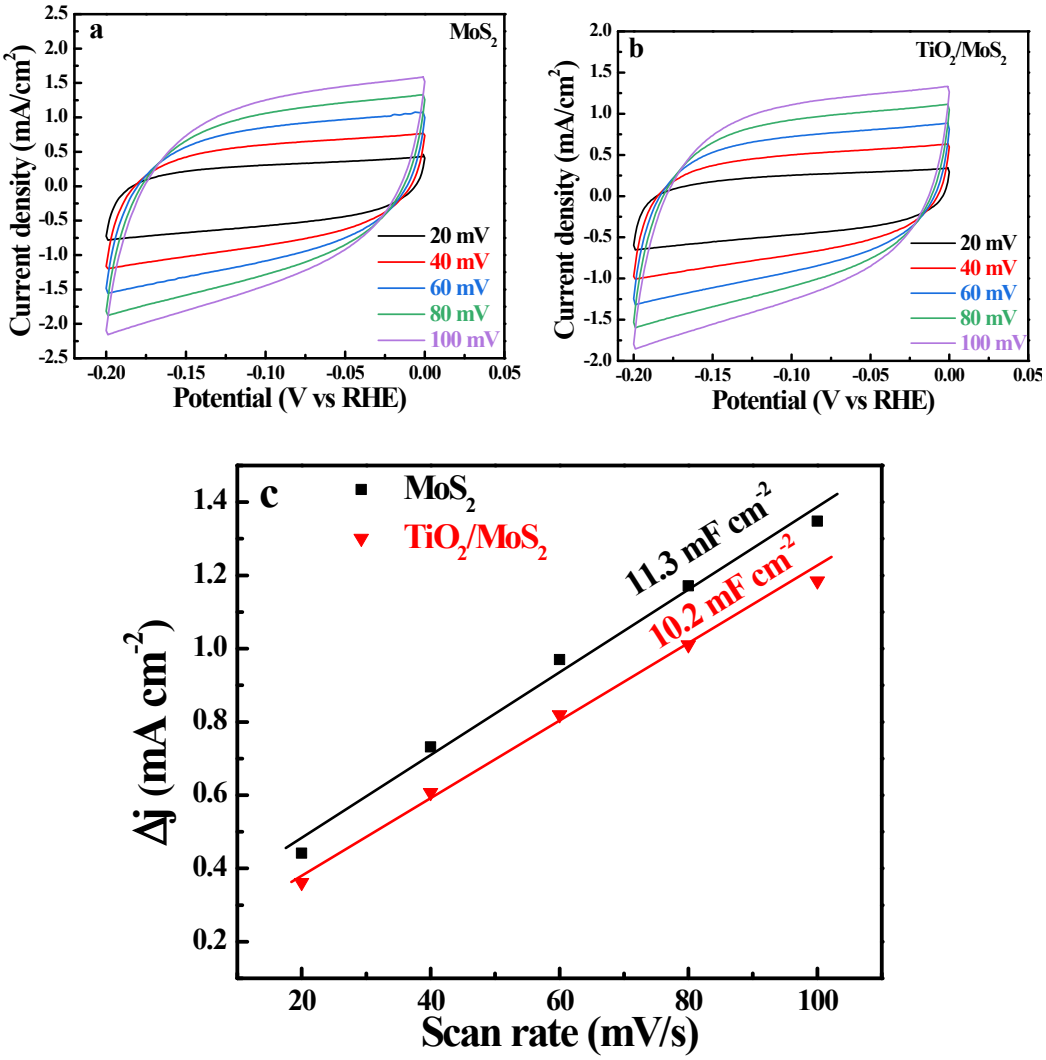

Fig. S6 CV curves of MoS_2 (a) and TiO_2/MoS_2 (b) performed at different scan rates. Charging current density differences plotted against scan rates (c).

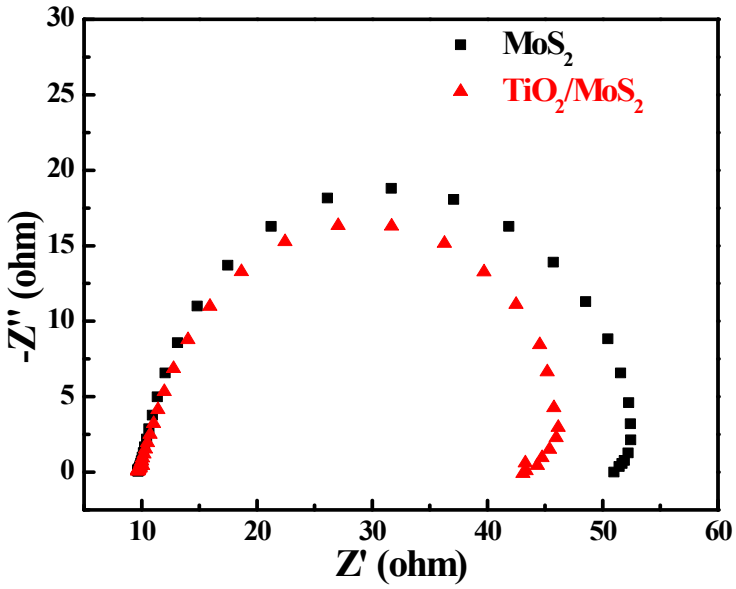

Fig. S7 EIS spectra of MoS_2 and TiO_2/MoS_2.

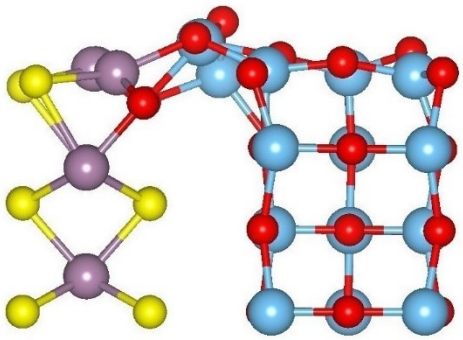

Fig. S8 Stable interfacial structure model of TiO_2/MoS_2.

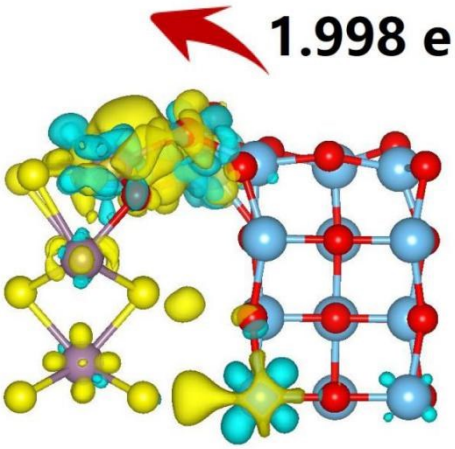

Fig. S9 Charge density difference and net Bader charge transfer of TiO_2/MoS_2.

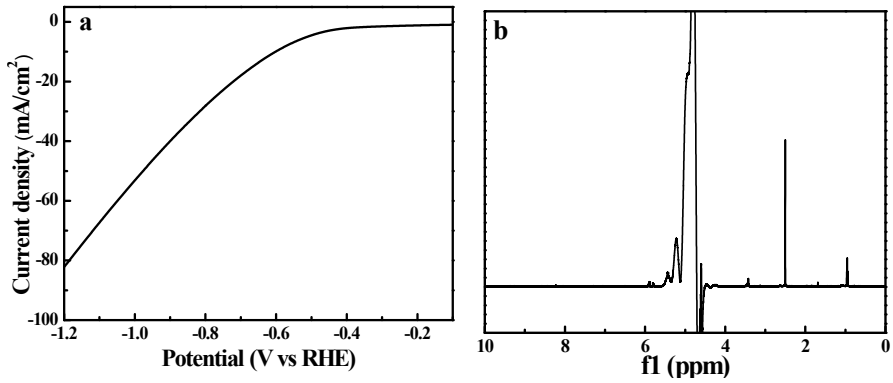

Fig. S10 LSV curve of TiO_2/MoS_2 in CO-saturated 0.5 M $KHCO_3$ aqueous solution (a). Corresponding ^1H NMR spectrum of liquid products (b).

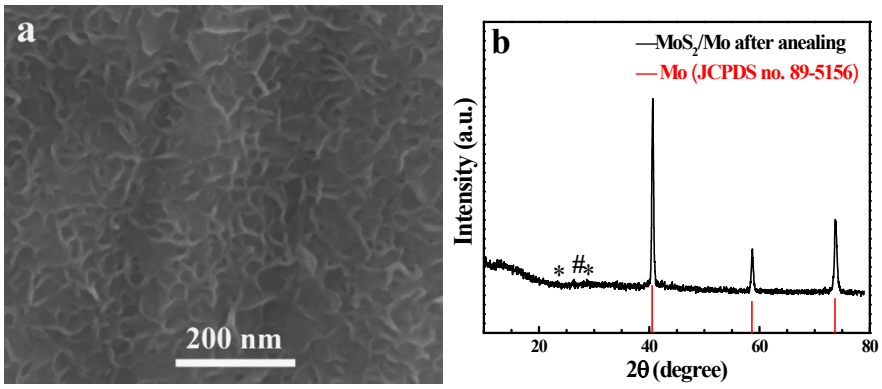

Fig. S11 FESEM image (a) and XRD pattern (b) of MoS_2 nanosheet arrays grown on Mo mesh after annealing in air at 300 °C for 4 h. * and # denote MoO_3 and MoO_2, respectively.

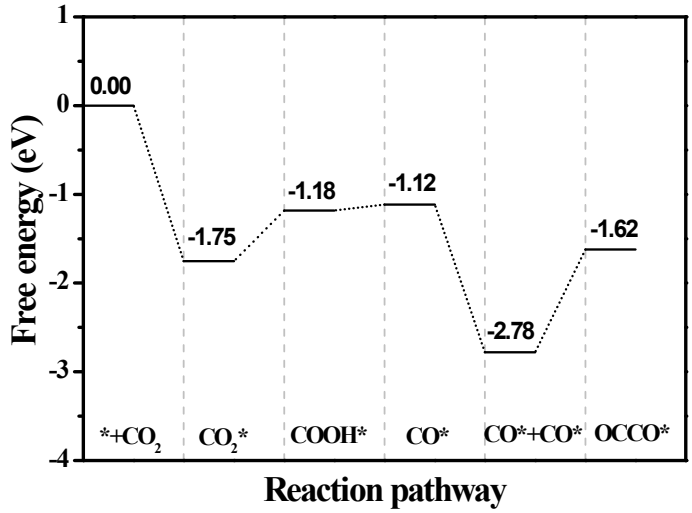

Fig. S12 Free energy diagrams for the coupling reaction of CO over MoS_2.

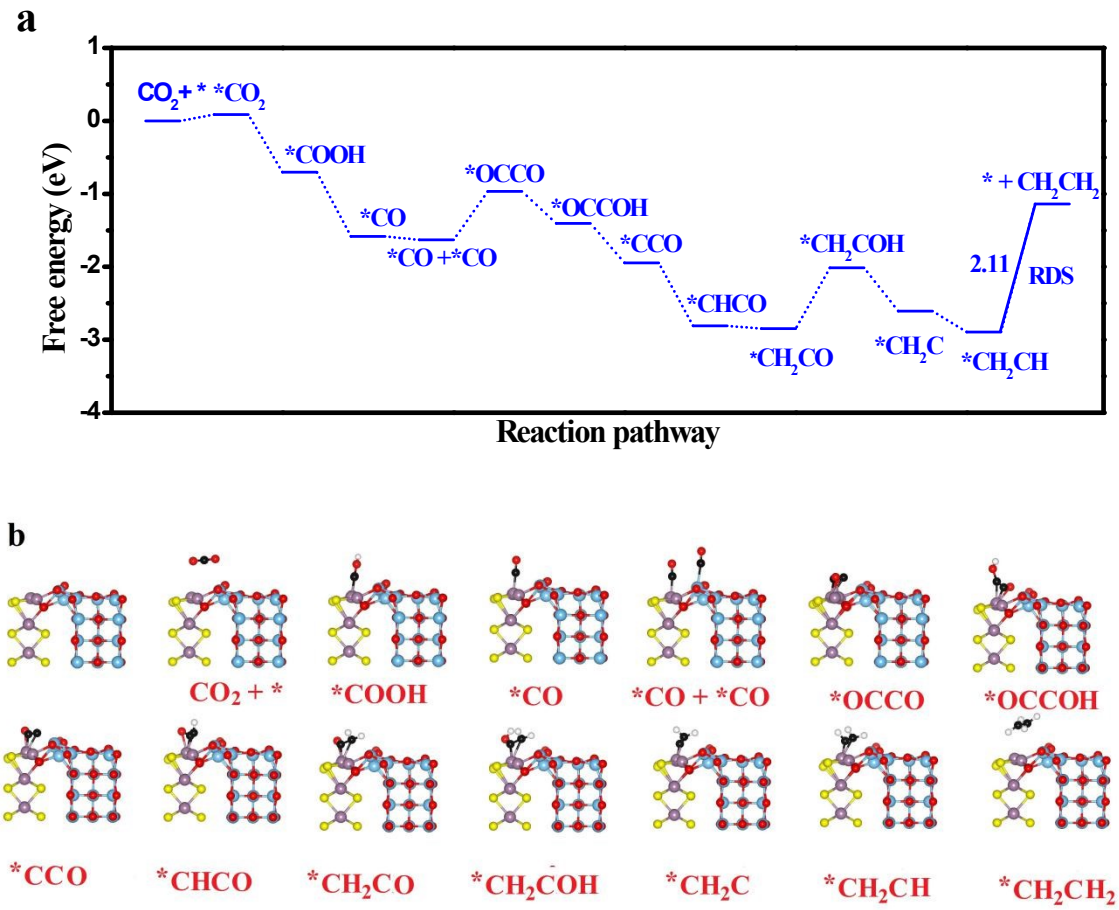

Fig. 13 Free energy diagrams for CO_2RR over TiO_2/MoS_2 toward ethylene (a). The optimized geometries for the reaction intermediates during the CO_2RR process to C_2H_4 over the interface of TiO_2/MoS_2 (b).

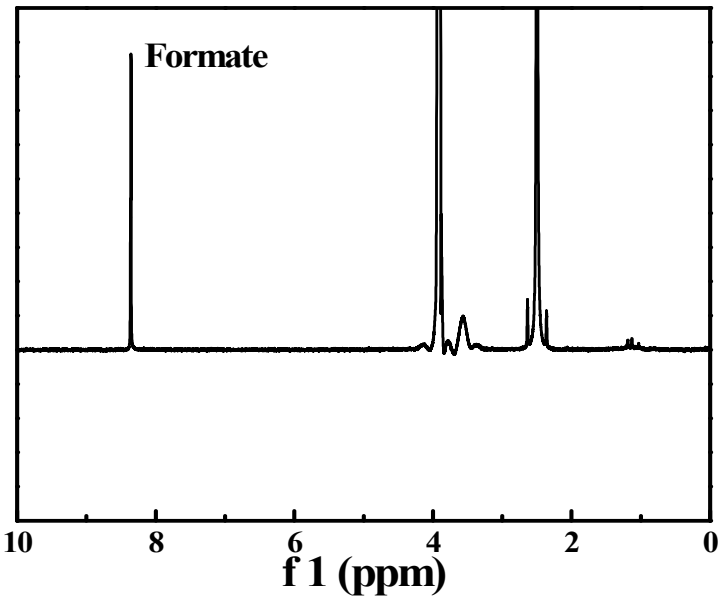

Fig. S14 ^{1}H NMR spectrum of liquid products obtained through CO_2 electrolysis over MoS_2 nanosheet arrays loaded by excess TiO_2.

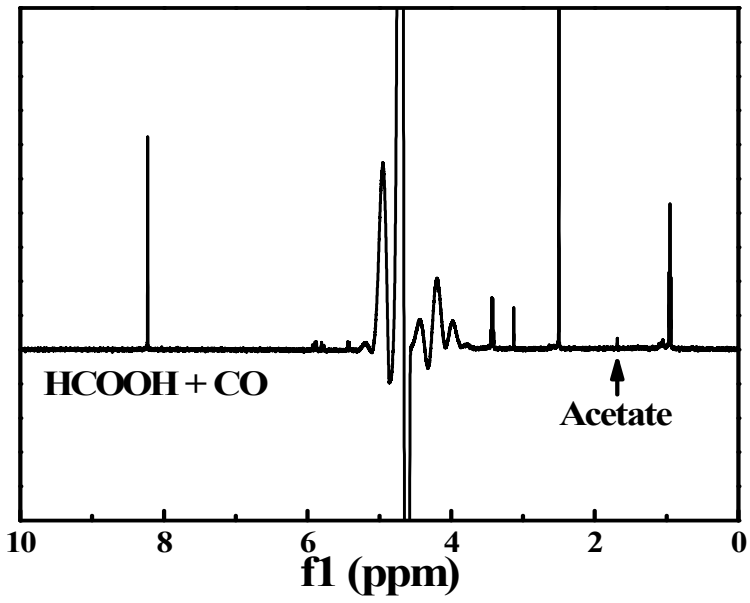

Fig. S15 ^{1}H NMR spectrum of liquid products obtained through CO electrolysis over TiO_2/MoS_2 nanosheet arrays in the presence of formate ions.

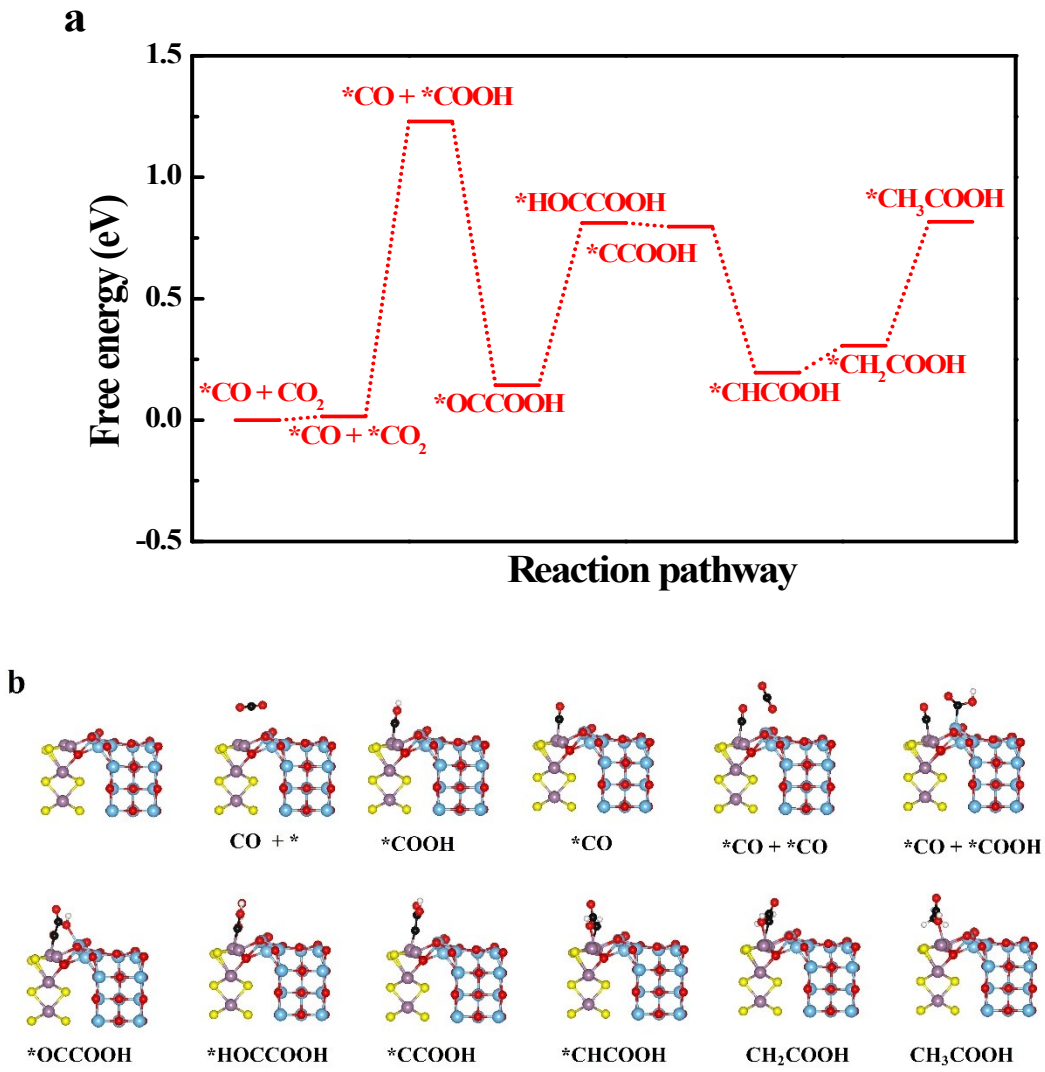

Fig. S16 Free energy diagrams for CO_2RR over TiO_2/MoS_2 toward acetate (a). The optimized geometries for the reaction intermediates during the CO_2RR process to CH_3COOH over the interface of TiO_2/MoS_2 (b).

Table S1. Comparison of electrocatalytic activity of different electrocatalysts for CO_2RR toward ethanol.

Catalysts	Reaction condition	FE (%)	Partial current density [mA cm^{-2}]	Reference
Cu nanoparticle ensembles	0.1 M $KHCO_3$, −0.86 V vs RHE	16.6	3.4	1
B doped Cu	0.1 M KCl −1.1 V vs RHE	27	18.9	2
Cu_4Zn	0.1 M $KHCO_3$ −1.05 V vs RHE	29.1	8.2	3
Cu-Au alloy	0.5 M $KHCO_3$ −1.1 V vs SCE	12	0.24	4
Phase-blended Ag-Cu_2O	0.2 M KCl −1.2V vs RHE	34.2	0.9	5
Cu/TiO_2	0.2 M KI −1.45 V vs. RHE	27.4	8.7	6
Cu_2S–Cu-V	0.1 M $KHCO_3$ −0.95 V vs RHE	15.1	4.8	7
Cu-C_3N_4	0.1 M $KHCO_3$ −1.6 V vs Ag/AgCl	10	0.8	8
Nitrogen-doped mesoporous carbon	0.1 M $KHCO_3$ −0.56 V vs RHE	77	0.5	9
B and N-co-doped nanodiamond	0.1 M $NaHCO_3$ −1.0 V vs RHE	93.2	0.6	10
TiO_2/MoS_2	0.5 M $KHCO_3$ −0.6 V vs RHE	50	1.2	This work

Reference

[1] D. Kim, C. S. Kley, Y. Li, P. Yang, *Proc. Natl. Acad. Sci*. **2017**, *114*, 10560–10565.

[2] Y. S. Zhou, F. L. Che, M. Liu, C. Q. Zou, Z. Q. Liang, P. D. Luna, H. F. Yuan, J. Li, Z. Q. Wang, H. P. Xie, H. M. Li, P. N. Chen, E. Bladt, R. Quintero-Bermudez, T. K. Sham, S. Bals, J. Hofkens, D. Sinton, G. Chen, *Nat. Chem*. **2018**, *10*, 974–980.

[3] D. Ren, B. S. H. Ang, B. S. Yeo, *ACS Catal*. **2016**, *6*, 8239−8247.

[4] F. L. Jia, X. X. Yu, L. Z. Zhang, *J. Power Sources* **2014**, *252*, 85–89.

[5] S. Lee, G. Park, J. Lee, *ACS Catal*. **2017**, *7*, 8594–8604.

[6] J. Yuan, L. Liu, R. R. Guo, S. Zeng, H. Wang, J. X. Lu, *Catalysts* **2017**, *7*, 220.

[7] T. T. Zhuang, Z. Q. Liang, A. Seifitokaldani, Y. Li , P. D. Luna, T. Burdyny, F. L. Che , F. Meng , Y. M. Min , R. Quintero-Bermudez, C. T. Dinh , Y. J. Pang, M. Zhong, B. Zhang, J. Li, P. N. Chen, X. L. Zheng, H. Y. Liang, W. N. Ge, B. J. Ye, D. Sinton, S. H. Yu, E.H. Sargent, *Nat. Catal*. **2018**, *1*, 421–428.

[8] Y. Jiao, Y. Zheng, P. Chen, M. Jaroniec, S. Z. Qiao, *J. Am. Chem. Soc*. **2017**, *139*, 18093−18100.

[9] Y. F. Song, W. Chen, C. C. Zhao, S. G. Li, W. Wei, Y. H. Sun, *Angew. Chem. Int. Ed*. **2017**, *56*, 10840–10844.

[10] Y. M. Liu, Y. J. Zhang, K. Cheng, X. Quan, X. F. Fan, Y. Su, S. Chen, H. M. Zhao, Y. B. Zhang, H. T. Yu, M. R. Hoffmann, *Angew. Chem. Int. Ed*. **2017**, *56*,15607–15611.